

pubs.acs.org/JPCA Article

Investigating Intramolecular H Atom Transfer Dynamics in β -Diketones with Ultrafast Infrared Spectroscopies and Theoretical Modeling

Jessika L.S. Dean,[§] Valerie S. Winkler,[§] Mark A. Boyer, Edwin L. Sibert III,* and Joseph A. Fournier*



Cite This: J. Phys. Chem. A 2023, 127, 9258–9272



ACCESS I

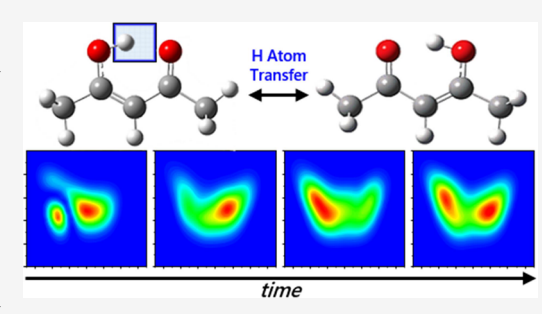
Metrics & More

Article Recommendations

Supporting Information

Transition State

ABSTRACT: The vibrational signatures and ultrafast dynamics of the intramolecular H-bond in a series of β -diketones are investigated with 2D IR spectroscopy and computational modeling. The chosen β -diketones exhibit a range of H atom donor—acceptor distances and asymmetry along the H atom transfer coordinate that tunes the intramolecular H-bond strength. The species with the strongest H-bonds are calculated to have very soft H atom potentials, resulting in highly red-shifted OH stretch fundamental frequencies and dislocation of the H atom upon vibrational excitation. These soft potentials lead to significant coupling to the other normal mode coordinates and give rise to the very broad vibrational signatures observed experimentally. The 2D IR spectra in both the OH and OD stretch regions of the light and deuterated



isotopologues reveal broadened and long-lived ground-state bleach signatures of the vibrationally hot molecules. Polarization-sensitive transient absorption measurements in the OH and OD stretch regions reveal notable isotopic differences in orientational dynamics. Orientational relaxation was measured to occur on $\sim\!600$ fs and $\sim\!2$ ps time scales for the light and deuterated isotopologues, respectively. The orientational dynamics are interpreted in terms of activated H/D atom transfer events driven by collective intramolecular structural rearrangements.

■ INTRODUCTION

Symmetric β -diketones, particularly malonaldehyde and acetylacetone, have served as popular models for experimental and computational studies on strong intramolecular H-bonds and H atom transfer dynamics. 1-5 For acetylacetone, microwave spectroscopy experiments suggested an equilibrium C_{2v} structure in which the H-bonded H atom is equally shared between the donor and acceptor oxygen atoms.⁶ This result sparked interest in high-level calculations on the energetics of the H transfer reaction coordinate. $^{4,5,7-11}$ Quantum chemical calculations consistently predict the C_{2v} structure to be a transition state between two equivalent C_s minima (see Figure 1). The transition barrier, however, is predicted to be quite low and is highly dependent on the level of theory and basis set size. Coupled-cluster calculations predict a H transfer barrier of \sim 3 kcal/mol (\sim 1100 cm⁻¹), with the inclusion of zero-point corrections lowering the barrier to only ~1 kcal/mol (~350 cm^{-1}). 10

A full-dimensional CCSD(T) potential energy surface (PES) for acetylacetone was recently reported by Kaser et al. using machine learning approaches starting from a lower-level MP2 surface. Using this PES, H atom residence times using classical molecular dynamics were reported. The simulations predicted that the majority of H transfer events occur within ~700 fs and are driven by motions in the low-frequency O–O H donor–acceptor mode. A full-dimensional CCSD(T) PES

$$\begin{array}{cccc}
H & C & C & H \\
H & H & H \\
R_1 & R_2
\end{array}$$

Minimum

 $(R_1, R_2) = (Ph, Ph), (CH_3, Ph), (CH_3, CH_3), (CH_3, CF_3), (CF_3, CF_3)$

Figure 1. Minimum-energy and transition-state structures of acetylacetone. Five variants were investigated, denoted by the identities of the $(R_1,\ R_2)$ end groups. The $\{x,\ y\}$ coordinate system that defines the H atom in-plane degrees of freedom is indicated in the minimum-energy structure.

Received: August 10, 2023
Revised: September 25, 2023
Accepted: October 10, 2023
Published: October 26, 2023





was also recently reported by Qu et al. using an alternative machine learning approach. In that report, the calculated ground-state tunneling splitting of $\sim\!38~{\rm cm}^{-1}$ inferred a H tunneling half-period of $\sim\!400~{\rm fs}~(\sim\!8~{\rm cm}^{-1}$ splitting, $\sim\!2~{\rm ps}$ tunneling half-period for the deuterated isotopologue). Interestingly, the calculated ground-state wave function of all H atoms indicated that the shared H atom was consistent with the C_s structure while the methyl H atoms were consistent with the C_{2v} arrangement. Low torsional barriers (<200 cm $^{-1}$) for rotation of the terminal methyl group nearest the H acceptor O atom (R_2 in Figure 1) have been predicted, 4,11 corroborating the experimental results determined from microwave spectroscopy. 6

The strong H-bond interactions and complicated anharmonic effects in β -diketones result in very broad and weak OH stretch vibrational features, which make infrared (IR) spectroscopic investigations and comparisons to computational predictions challenging. Ultrafast transient absorption (TA) and two-dimensional (2D) IR spectroscopies have provided important fundamental insight into strong H-bond interactions and vibrational dynamics within both intramolecular 13-15 and intermolecular 16-29 H-bond model systems. Fast vibrational lifetime dynamics (<300 fs) are typically observed, consistent with strong anharmonic coupling and relaxation of OH/NH stretches to other modes. Indeed, 2D IR spectra have revealed intense off-diagonal cross-peaks between OH/NH stretches and lower-frequency fingerprint modes within model systems.²² Prominent modulations in OH/NH stretch transitions with pump-probe delay time have also been observed, consistent with coherent coupling to or impulsive excitation of the low-frequency H atom donor-acceptor modes. 13-17

We recently reported TA and 2D IR spectra of acetylacetone in the OH bend and stretch regions.³⁰ The OH bend exhibited a strong, broad cross-peak to the other fingerprint modes, indicating significant OH bend character throughout the fingerprint region. A highly elongated bend overtone induced absorption feature suggested the presence of significant bendstretch coupling. The OH and OD stretch regions in the light and deuterated isotopologues, respectively, revealed homogeneously broadened ground-state bleach absorptions with minimal dynamics beyond 100 fs. The constant bleach signals indicated that acetylacetone remained vibrationally hot following excitation and subsequent vibrational relaxation to lower-frequency modes. Unlike previously studied model systems, low-frequency modulations were not observed in the TA signals. Interestingly, orientational relaxation dynamics, measured using polarization-sensitive TA, persisted well beyond the vibrational lifetimes and displayed significant isotopic differences.

Herein, we report TA and 2D IR spectra for the series of β -diketones shown in Figure 1, in which the identities of the terminal groups R_1 and R_2 are varied (Ph, CH₃, or CF₃). The H-bond strengths range from nearly barrierless transfer potentials to more conventional H-bonds. The species with mixed substituents further introduce asymmetry into the H transfer PES. Like acetylacetone, long-lived and isotopic-dependent polarization anisotropy dynamics were measured. The exception was the biphenyl derivative, which displayed relatively fast (200 fs) anisotropy decays in both isotopologues. The other models displayed similar anisotropy decay time scales, with the OH stretches decaying within \sim 600 fs and the OD stretches within \sim 2 ps. The similar time scales suggest a common mechanism at play for loss of the initial orientational

memory. We interpret the orientational dynamics in terms of H/D atom transfer events that involve large internal structural rearrangements that stabilize the transfer products. We also present computational modeling of the two-dimensional inplane H atom PESs. The calculated soft potentials result in various degrees of delocalization of the H/D atom between the donor and acceptor groups upon vibrational excitation, as well as coupling to the other normal mode coordinates. Short-time dynamics calculations reveal ultrafast vibrational relaxation time scales and large-amplitude H atom motions. Together, these results offer new insights into the origins of the broad vibrational spectral signatures and dynamics of strongly shared intramolecular H atoms.

■ EXPERIMENTAL METHODS

The output of a regenerative amplifier (Coherent Astrella, 800 nm, 30 fs, 1 kHz, 3.6 mJ/pulse) pumped a commercial optical parametric amplifier (Light Conversion, TOPAS Prime) to generate tunable near-IR signal (1.3–1.45 $\mu \rm m)$ and idler (1.8–2.1 $\mu \rm m)$ beams. The signal and idler beams were combined in a 1 mm thick AgGaS $_2$ crystal (Eksma Optics) in a home-built difference frequency generation setup 31 resulting in IR pulses tunable between 3 and 7 $\mu \rm m$. IR pulse bandwidths were between 200 and 300 cm $^{-1}$ with pulse widths of about 80 fs measured with interferometric autocorrelation.

The IR pulse was first sent through a 1 mm wedged CaF_2 window to generate a probe pulse from the reflection off of the front face of the window (~1% reflection) and a reference pulse from the reflection off the wedged back face. The probe pulse was directed to a translation stage (Aerotech; ANT95L050-MP-PL2-TAS) to control the pump—probe delay time τ_2 . The reference pulse was directly routed to the MCT detector. A pump pulse pair was generated and controlled by a mid-IR pulse shaper³² (PhaseTech). The pump and probe pulses were directed and focused (~100 μ m spot size) into the sample in the pump—probe geometry, generating a signal field that was self-heterodyned by the probe pulse. The probe and reference lines were dispersed by a monochromator onto a 128 × 128 pixel MCT focal-plane array detector (PhaseTech), generating the ω_3 detection axis.

For each ω_3 probe frequency at a given pump-probe delay time τ_2 , the TA signal was recorded for pump pulse i as $-\log[(S_i/R_i)/(R_{i+1}/S_{i+1})]$, where S is the signal monitored by the probe and R is the reference pulse. Reported TA spectra collected near 3 μ m were collected with the following τ_2 step sizes: -500 to -250 fs in steps of 50 fs, -200 to 500 fs in steps of 20 fs, 550 fs to 1.5 ps in steps of 50 fs, and 1.6 to 5 ps in steps of 100 fs. Reported TA spectra collected near 5 μ m were collected with the following τ_2 step sizes: -500 to -250 fs in steps of 50 fs, -200 to 500 fs in steps of 20 fs, 550 fs to 1.5 ps in steps of 50 fs, and 1.6 to 8 ps in steps of 100 fs. The polarization of the probe pulse was controlled using a CdSe zero-order half-wave plate (Alphalas; PO-TWP-L2-25-FIR) and ZnSe polarizer (Edmund Optics; model 62-772). All TA spectra presented in the main text were collected at magic angle polarization. For anisotropy measurements, ZZZZ and ZZYY TA spectra were collected separately, making sure that pump powers and late-time TA signals were the same in both schemes. Anisotropy was calculated as $(I_{par} - I_{perp})/(I_{par} +$

 $\dot{2}\dot{D}$ spectra were generated by monitoring the TA signal at each ω_3 pixel as a function of the pump pair delay time τ_1 , the Fourier transform of which yielded the ω_1 excitation axis. All

reported 2D IR spectra were collected at magic angle polarization. In the 5 μ m region, a τ_1 step size of 8 fs was used with a rotating frame 32 of 800 cm $^{-1}$, while a step size of 8 fs with a rotating frame of 1750 cm $^{-1}$ was used when pumping near 3 μ m. The τ_1 free-induction decay at each ω_3 pixel was first apodized with a Hanning window and zero-padded to twice the number of points collected for a line spacing of about 16-20 cm $^{-1}$ along ω_1 . The data were interpolated to 1 cm $^{-1}$ spacing over ω_1 and ω_3 . All 2D IR spectra were normalized to 1 with red features corresponding to ground-state bleach signals and blue features corresponding to excited-state/induced absorption signals.

All studied β -diketones were purchased from Sigma-Aldrich and used without further purification. The preparation of d₂-(CH₃, CH₃) was described in our previous publication.³⁰ Deuteration of (Ph, Ph) and (Ph, CH₃) was done by refluxing the nondeuterated molecule in D₂O (in a 1:30 solution) for 4 h at 100 °C. The organic phase was then extracted using ethyl acetate and the solvent was removed under vacuum. The preparation of d₂-(CH₃, CF₃) was done by refluxing trifluoroacetylacetone in D₂O (1:3) for 4 h at 100 °C. The organic phase was then extracted using a glass pipet. FTIR spectra confirmed complete exchange of the labile protons. Samples were sandwiched between two 1 mm CaF₂ windows using a 125 μ m Teflon spacer in a home-built sample cell. Due to strong background CHCl₃ absorption near 3000 cm⁻¹, OH stretch data were collected from 0.7 M samples in CDCl₃ using a 300 μ m spacer.

■ COMPUTATIONAL METHODS

The computational strategies were described in more detail previously, $^{33-36}$ and will be briefly summarized here. The positions of all atoms except for the shared H atom were described using the Z-matrix coordinate representation. The shared H atom was described by the Cartesian coordinates $\{x, y, z\}$ based on a localized reference frame relative to the positions of the remaining atoms. The x-axis lies along the donor—acceptor axis with the origin at the midpoint between these two atoms. The y-axis is perpendicular to the x-axis and lies in the plane defined by the O and C atoms directly below the donating O atom (see Figure 1). The z-axis follows directly from these two definitions.

The Wilson F and G matrices³⁷ were then calculated at the equilibrium configuration, where the F matrix was calculated from the Hessian obtained in a *Gaussian* frequency calculation.³⁸ All calculations were carried out at the B3LYP/6-311++G(d,p) level of theory. The $\{x,y\}$ degrees of freedom were decoupled from the remaining internal degrees of freedom by zeroing the appropriate elements of the F and G matrices. Diagonalizing these two matrices leads to a set of normal coordinates that, when combined with the $\{x,y\}$ coordinates, fully describe the internal degrees of freedom.

The potential was expanded in terms of the normal coordinates to second order as

$$V = V_0 - \mathbf{f}^T \mathbf{Q} + \frac{1}{2} \mathbf{Q}^T \mathcal{F} \mathbf{Q}$$
 (1)

where $\{V_0, \mathbf{f}, \mathcal{F}\}$ are the potential, forces, and force constant matrix written as functions of x and y when all remaining coordinates are held at their equilibrium values. The dipole and its derivatives were calculated as $\mathbf{d} = \mathbf{d}_0 + \mathbf{D}^T \mathbf{Q}$, where $\{\mathbf{d}_0, \mathbf{D}\}$ are the dipole components and their derivatives calculated in an Eckart frame. The $\{x, y\}$ dependencies of these potential

parameters were modeled on a grid of points that were used as input for a discrete variable representation (DVR) calculation.

The full Hamiltonian takes the form $\hat{H} = \hat{T} + \hat{V}$, where the potential is given by eq 1. The coordinate choice leads to a simple approximate form for the kinetic energy contribution:

$$\widehat{T} = \frac{1}{2} [G_{xx} p_x^2 + G_{yy} p_y^2] + \frac{1}{2} \sum_i P_i^2$$
(2)

where P_i are the normal coordinate momenta. The kinetic contribution was treated at the harmonic level, and the coordinate dependencies of the Wilson G-matrix elements were ignored. The kinetic coupling of the $\{x, y\}$ degrees of freedom to the other vibrational coordinates was also neglected. This coupling is small due to the light proton and the choice of the $\{x, y\}$ internal coordinates.

The contributions that depend solely on the $\{x, y\}$ degrees of freedom were used to define the H atom Hamiltonian:

$$\widehat{H}^{x,y} = \frac{1}{2} [G_{xx} p_x^2 + G_{yy} p_y^2] + V_0$$
(3)

The associated eigenfunctions (Ψ_n) and eigenvalues were solved using a sinc DVR³⁹ based on a 35 × 23 grid of $\{x, y\}$ points. Only those ~600 points for which V_0 was less than 19,000 cm⁻¹ were included in the 2D-DVR calculations. Based on previous studies, the number of grid points used is expected to yield eigenvalues that are accurate to 1 cm⁻¹ for the 10 lowest states.

In order to include the coupling between the $\{x,y\}$ degrees of freedom and the remaining normal modes, which is described in the second two terms of eq 1, the final Hamiltonian was setup as a direct product of N of the lowest-energy eigenfunctions described above and a harmonic oscillator basis $|v\rangle$ describing a subset K of the \mathbf{Q} degrees of freedom. For a given subset K, the normal modes chosen for inclusion in the basis were selected as follows. The value f_i^2/\mathcal{F}_{ii} was evaluated in wavenumbers at the midpoint for the K atom transfer. The K-1 normal modes with the largest value of this metric were included in addition to the normal mode which closely approximated the out-of-plane OH motion.

The product form of the potential in eq 1 leads to easy evaluation of the matrix elements. The size of the harmonic oscillator basis |v| was controlled by a single parameter M. Only those basis functions for which $\sum_i v_i$ is less than M were included in the basis. The Hamiltonian in the $|\Psi_n\rangle|v\rangle$ basis has many zero elements and is ideal for iterative methods for solving the Schrödinger equation. To obtain vibrational spectra, the three-stage approach of Stanton was followed.⁴⁰ First, the Davidson method⁴¹ was used to calculate the groundstate eigenfunction, $|\Phi_{gs}\rangle$, of the full Hamiltonian as a linear combination of the basis $|\Psi_n\rangle|\mathbf{v}\rangle$. We next evaluated $d_x|\Phi_{gs}\rangle$ and $d_v | \Phi_{gs} \rangle$, where d_x and d_v are the in-plane components of the dipole. The d_x and d_y vectors were the starting vectors of the Lanczos method, 42 which, as an output, provides the eigenvalues Ek and the eigenfunction expansion coefficients $A_{\alpha,k} = \langle \Phi_k \mid d_\alpha \mid \Phi_{gs} \rangle$. The spectral intensities were calculated

$$I_{k} = (A_{x,k}^{2} + A_{y,k}^{2})E_{k} \tag{4}$$

The z-components of the dipole were included in initial studies, but their contribution to the spectra under consideration was found to be negligible.

Short-time dynamics were investigated via numerical solutions of the time-dependent Schrödinger equation

$$\Psi(x, y, \mathbf{Q}, t) = \sum_{n} \sum_{\mathbf{v}} c_{n, \mathbf{v}}(t) |\Psi_{n}\rangle |\mathbf{v}\rangle$$
(5)

using the method of Askar and Cakmak⁴³ in which the coefficients evolve as

$$\mathbf{c}(t + \Delta t) = \mathbf{c}(t - \Delta t) - 2i\Delta t \mathbf{H} \mathbf{c}(t)$$
 (6)

Time steps of 0.033 fs were employed.

The time-dependent approach allows us to connect with the classical ideas of energy transfer. If a specific state of the $\{x, y\}$ degrees of freedom $|\Psi_n\rangle|v\rangle$ were excited, time-dependent models can be used to follow the time evolution of this state and determine where energy flows in the molecule. Following ideas based on density matrices, integration over the ${\bf Q}$ degrees of freedom yields

$$P(x, y) = \int d\mathbf{Q} |\Psi(x, y, \mathbf{Q}, t)|^{2}$$
$$= \sum_{n} \sum_{m} d_{m,n} \Psi_{m}^{*}(x, y) \Psi_{n}(x, y)$$
(7)

where the diagonal elements $P_n = d_{n,n}$ are the probabilities of being in a given state $|\Psi_n\rangle$ of the $\{x,y\}$ degrees of freedom of the system.

For the calculations presented that involved rotation of the methyl groups to the transition-state geometry, a more advanced approach was taken in the potential expansion described in eq 1. This approach ensured that the potential was symmetric and equally accurate for both the H atom transfer reactant and product equilibrium structures such that the longer-time dynamics did not bias one structure over the other. A detailed description of this approach is provided in the Supporting Information.

RESULTS AND DISCUSSION

Harmonic Calculations. A summary of the harmonic calculation results for each species is given in Table 1, with

Table 1. Calculated H Atom Donor-Acceptor Distances (d_{OO}) and OH/OD Stretch Frequencies for the Five Studied Species^a

		OH stretc	h/cm ⁻¹	OD stretch/cm ⁻¹		
species	$d_{OO}/\textrm{Å}$	harmonic	model	harmonic	model	
(Ph, Ph)	2.50	2922	1885	2142	1603	
(CH ₃ , Ph)	2.52	3012	2142	2204	1754	
(CH_3, CH_3)	2.54	3066	2372	2243	1895	
(CH_3, CF_3)	2.58	3230	2752	2357	2027	
(CF ₃ , CF ₃)	2.59	3282	2810	2392	2063	

"Harmonic frequencies are unscaled. Model frequencies are those found by using the anharmonic computational approaches described in the text. All calculations were performed at the B3LYP/6-311++G(d,p) level and basis set.

optimized structures presented in Figure S1. The O–O distance (d_{OO}) and H atom transfer barrier height for acetylacetone, hereafter referred to as (CH_3, CH_3) , are 2.54 Å and 806 cm⁻¹, respectively, at the B3LYP/6-311++G(d,p) level and basis set. B3LYP and MP2 calculations tend to predict ~1.5 times smaller barriers and slightly shorter d_{OO} compared to coupled-cluster approaches for (CH_3, CH_3) . For

comparison, high-level calculations by Howard et al. 10 predicted $d_{OO} = 2.53 \text{ Å}$ and a barrier of 760 cm⁻¹ using MP2/aug-cc-pVTZ, while CCSD(T)/cc-pVTZ calculations predicted $d_{OO} = 2.55 \text{ Å}$ and a barrier of 1120 cm⁻¹. (Ph, Ph) is predicted to have the strongest H-bond and the smallest barrier. The minimum-energy structure for (CH₃, Ph) is predicted to be the isomer with the H atom bonded to the oxygen nearest the methyl group. The isomer where the H atom is bonded to the oxygen nearest the phenyl group is predicted to lie only ~200 cm⁻¹ higher in energy. For (CH₃, CF₃), the isomer with the H atom bound nearest the methyl group is predicted to be \sim 500 cm⁻¹ lower than that with the H atom bound nearest the CF₃ group. (CH₃, CF₃), therefore, exhibits the most asymmetric H transfer PES. Finally, (CF₃, CF₃) is predicted to have the weakest H-bond, highest OH stretch frequency, and largest barrier in the model series.

H Atom Potential and Anharmonic Predictions for (CH_3, CH_3) . The two-dimensional potential describing the inplane $\{x, y\}$ H atom degrees of freedom for (CH_3, CH_3) is presented in Figure 2. Although the full H atom transfer

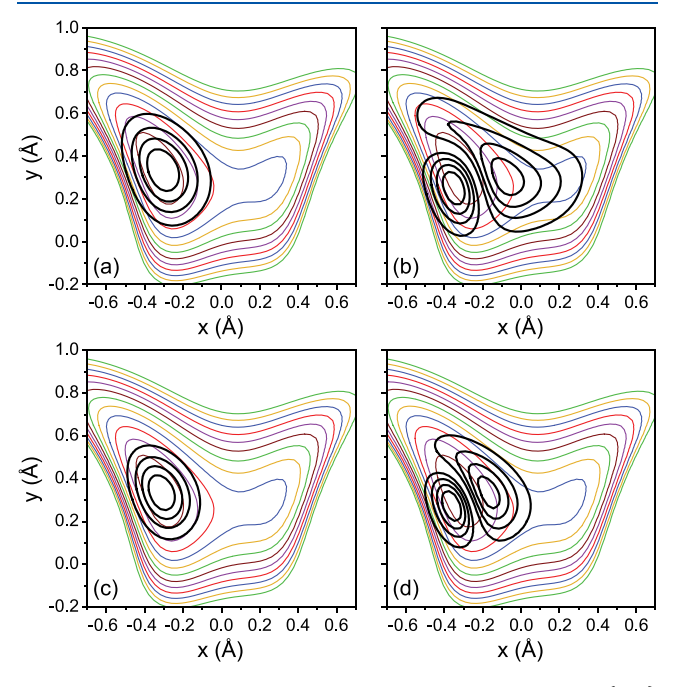


Figure 2. Equipotential curves for V_0 in eq 1 as a function of the $\{x,y\}$ coordinates for the H atom in (CH_3, CH_3) with all other atoms held fixed at their equilibrium positions. Contours are spaced by 1000 cm⁻¹ intervals. H and D atom wave functions are superimposed on the potential. (a) Ψ_1 H atom ground state. (b) Ψ_3 H atom state corresponding to one quantum in the OH stretch. (c) Ψ_1 D atom ground state. (d) Ψ_3 D atom state corresponding to one quantum in the OD stretch. The Ψ_3 states show significant bending character and dislocation across the transfer coordinate.

potential $(C_s-C_{2v}-C_s)$ is symmetric, scanning the shared H atom with all other atoms held fixed at their equilibrium C_s positions creates a localized potential that is not symmetric. The two-dimensional H atom potential is quite shallow along the H transfer coordinate, with a local minimum at the accepting O atom site that is ~4000 cm⁻¹ higher in energy than the global minimum position. The calculated ground-state H atom wave function (Ψ_1) is superimposed on the PES in Figure 2a and shows large amplitude along both the bending and stretching coordinates. The zero-point energy is ~2100

cm⁻¹. The Ψ_3 wave function is shown in Figure 2b and nominally represents one quantum of excitation in the OH stretch. The Ψ_3 wave function, however, displays significant amplitude along the OH bending coordinate, demonstrating strong mixing between the OH bending and stretching degrees of freedom. Importantly, amplitude extends across the transfer coordinate, indicating dislocation of the H atom between the donor and acceptor sites upon vibrational excitation of the Ψ_3 state. The Ψ_1 and Ψ_3 states for the D atom in the deuterated isotopologue are presented in Figure 2c,d, respectively. While more localized compared to the lighter H atom (zero-point energy ~1500 cm⁻¹), the Ψ_3 D atom wave function still shows appreciable amplitude that extends toward the transfer midpoint. The wave functions for additional H and D atom eigenstates are provided in Figures S2 and S3, respectively. The transition energies between the Ψ_1 and Ψ_3 states are about 2400 and 1900 cm⁻¹ for the light and deuterated isotopologues, respectively.

We repeated the above calculations using the CCSD(T) potential of Qu et al., ¹² which are presented in the Supporting Information. The CCSD(T) barrier is about 1000 cm⁻¹ higher in energy compared to the B3LYP prediction along the lowest-energy pathway between the donor and acceptor sites (Figure S4). This higher barrier results in a less, but still considerably, delocalized Ψ_3 OH stretch wave function (Figure S5). The predicted OH stretch frequency with the CCSD(T) potential increases by about 250 to ~2600 cm⁻¹. While the B3LYP barrier is too low, the presented calculations allow for the prediction of trends between the studied species and provide sufficient insight to guide analysis and interpretation of the experimental data.

The experimental infrared spectra of the light and deuterated isotopologues of (CH₃, CH₃) are presented in Figure 3a,c, respectively. Weak, broad, and substructured features between 2200 and 3000 cm⁻¹ in (CH₃, CH₃) and 1900-2200 cm⁻¹ in d₂-(CH₃, CH₃) are attributed to the OH and OD stretches, respectively. The broad nature of both features suggests significant anharmonic effects arising from the strong intramolecular H-bond. The model Hamiltonian discussed above that couples the H atom $\{x, y\}$ degrees of freedom to the other normal mode coordinates was used to see how the soft H atom potential influences the vibrational spectrum. The calculated vibrational spectra for the light and deuterated isotopologues are presented in Figure 3b,d, respectively. The calculation parameters used for both isotopologues were $\{M, N, I, K\} = \{4, \}$ 10, 600, 16}. M is the size of the harmonic oscillator (normal mode) basis such that only those basis functions for which $\sum_{i} v_{i} < M$ are included, where v_{i} are the normal mode quantum numbers. N is the number of H atom eigenstates. I is the number of Lanczos iterations. *K* is the number of normal mode coordinates. Note that the 16 normal modes included in the harmonic basis are nearly half of the total number of normal mode coordinates (39). The calculations predict considerable dilution of the oscillator strength derived from the OH and OD stretch modes over a large density of background states that arise from the harmonic basis. The calculated spectra show good general agreement with experiment, qualitatively predicting the overall spectral breadth in both isotopologues. The calculations highlight the complicated nature of the OH and OD stretch regions in strongly Hbonded systems and add to the growing number of systems where coupling of the H atom degrees of freedom to numerous

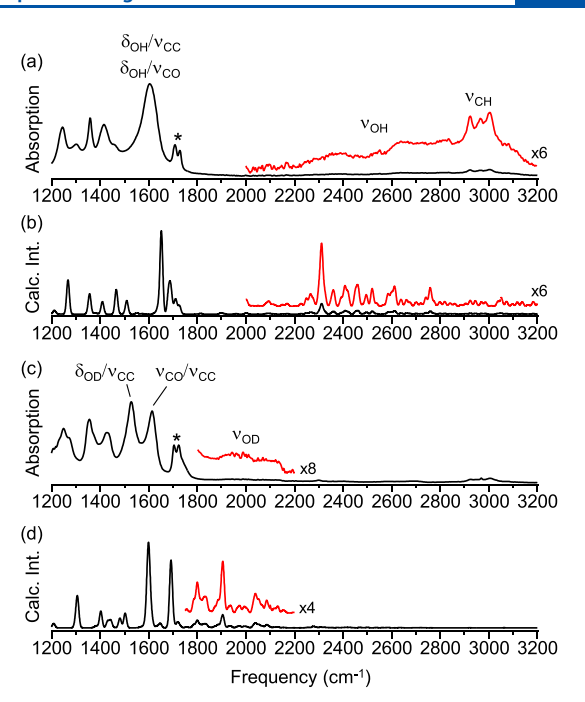


Figure 3. FTIR spectra for the neat liquids of (a) (CH₃, CH₃) and (c) d₂-(CH₃, CH₃). The broad and weak OH and OD stretch regions are colored red and are expanded for better visualization. The strongest transitions near 1600 cm⁻¹ derive from admixtures of the OH/OD bend ($\delta_{\rm OH}$, $\delta_{\rm OD}$), carbonyl stretch ($\nu_{\rm CO}$), and C=C stretch ($\nu_{\rm CC}$). Bands labeled with asterisks are from carbonyl stretches of the ketone isomer. Anharmonic predictions from the computational approach described in the text are provided in parts (b) and (d) for the light and deuterated isotopologues, respectively. The calculations qualitatively reproduce the experimentally observed breadths of the OH and OD stretch regions.

normal mode coordinates is necessary to understanding broad experimental spectra. 34,44

2D IR Spectra and Vibrational Dynamics. (CH3, CH3). The coupling of the OH/OD vibrational modes to a large basis of normal modes manifests in the 2D IR spectra of (CH₃, CH₃) as broad ground-state bleach signals (Figure 4a,b). The bleaches show no inhomogeneous broadening along the diagonal, and there is no evidence of induced overtone transitions, even at the earliest pump-probe waiting time (150 fs). The softness of the H atom $\{x, y\}$ potential leads to significant red-shifting of the nominal overtone transitions, which are predicted to occur near 700 and 850 cm⁻¹ along the probe axis for the light and deuterated isotopologues, respectively. Given the mixed bend-stretch character of the H atom wave functions, however, the description of these eigenstates as overtones is qualitative at best. With the complicated degree of mode mixing predicted within the OH and OD stretch regions, which includes coupling between the H atom eigenstates themselves, and rapid vibrational relaxation, it is difficult to predict if an overtone-like induced absorption would even be present experimentally. Previous studies on H-bond model systems by Petersen²² and Khalil⁴⁵ using broadband IR probe sources also failed to detect unambiguous signatures of induced overtone transitions. There is, however, a significant bleach signal intensity appearing off the diagonal spanning both the pump and probe axes. The light isotopologue, in particular, shows a strong bleach signal toward lower pump frequencies indicating a cross-peak-like feature between the higher and lower frequency regions of the

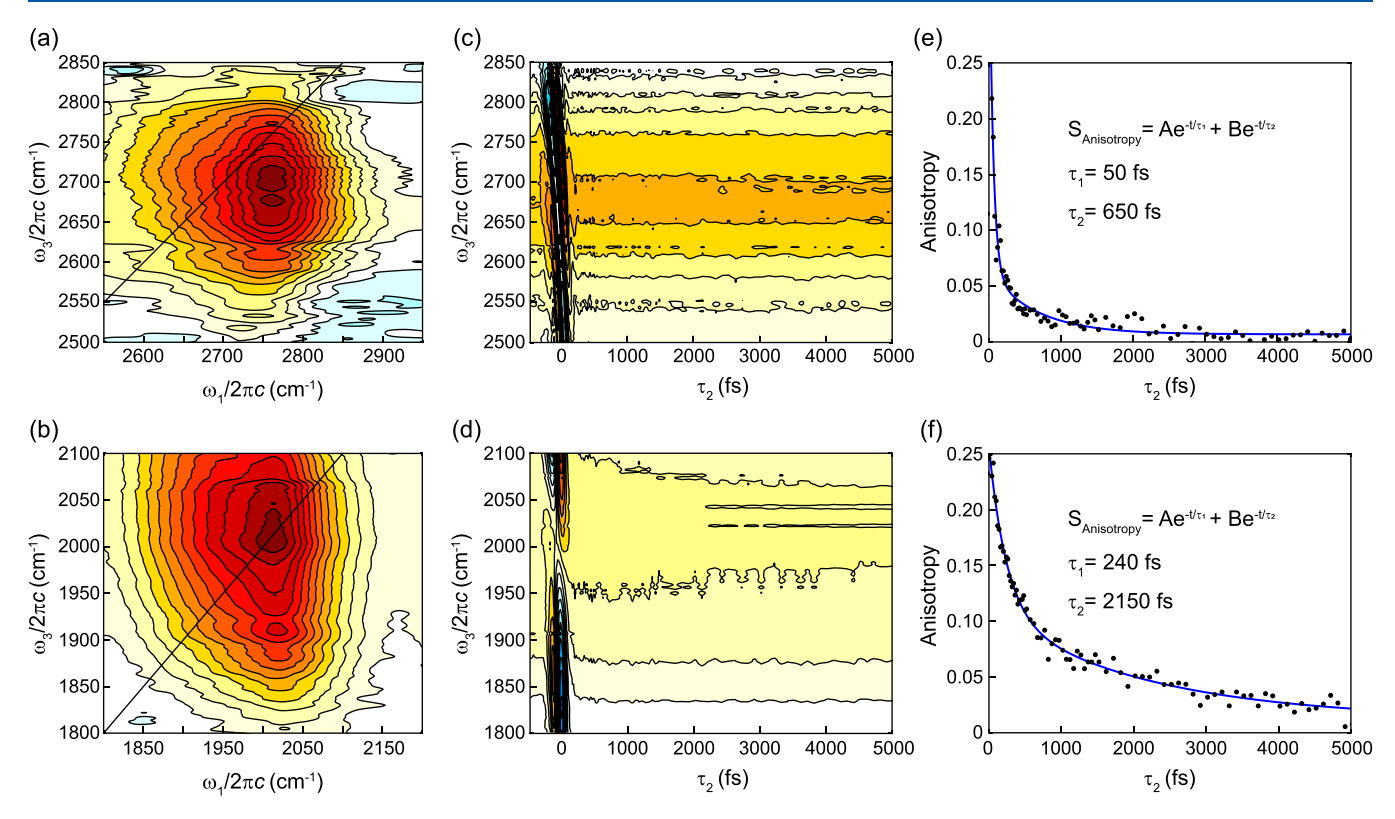


Figure 4. Isotropic 2D IR spectra collected at 150 fs waiting time for (a) (CH_3, CH_3) in the OH stretch region and (b) d_2 - (CH_3, CH_3) in the OD stretch region. Both spectra reveal homogeneously broadened ground-state beach signals. Isotropic TA spectra for (c) (CH_3, CH_3) and (d) d_2 - (CH_3, CH_3) show that the bleach signals are long-lived with minimal dynamical evolution. Polarization anisotropy measurements for (e) (CH_3, CH_3) and (f) d_2 - (CH_3, CH_3) show relatively long-lived orientational dynamics. Time constants for the biexponential fits of the anisotropy data are provided in the figures and are summarized in Table 2.

broad OH stretch transition (Figure 3a). The broad bleach signals highlight the strong mixing and dilution of the OH/OD stretches throughout these spectral regions anticipated by the computational predictions presented in Figure 3b,d.

Isotropic TA spectra for the light and deuterated isotopologues of (CH₃, CH₃) are shown in Figure 4c,d, respectively. At pump-probe delays beyond the pulse overlap region (~150 fs), the bleach signals remain at nearly constant intensity through the latest waiting time measured (Figure S6). The long-lived bleach signals indicate that recovery of the overall vibrational ground state through dissipation of the excitation energy to the solvent takes place on much longer time scales. (CH₃, CH₃), therefore, remains vibrationally hot over the experimental waiting time period as the excitation energy relaxes into the coupled lower-frequency normal mode coordinates. The lack of recovery of the OH/OD stretch ground state further indicates the strong dependence of the OH/OD stretch coordinate on the other normal modes. There is also no evidence of frequency shifting of the OH/OD stretch manifold, suggesting that the average H-bond strength is neither weakening nor strengthening upon relaxation of the vibrational energy in the lower-frequency coordinates. Interestingly, low-frequency modulations in the OH or OD stretch TA signals are not clearly evident. The dependence of the OH/OD stretch on many normal mode coordinates, not just the O-O mode, likely rapidly washes out any coherent coupling signatures.

Although the isotropic TA signals show little dynamical evolution, polarization-sensitive TA measurements reveal relatively long-lived anisotropy decay time scales. For the

OH stretch in (CH_3, CH_3) , the anisotropy shows biexponential decay behavior with a major sub-100 fs component (0.85 amplitude) that occurs within the pulse overlap region followed by a minor component (0.15 amplitude) that decays with a \sim 650 fs time constant (Figure 4e). The OD stretch anisotropy, on the other hand, decays over longer time scales with an initial \sim 250 fs fast component (0.6 amplitude) and a \sim 2200 fs slow component (0.4 amplitude).

It is instructive to discuss the possible physical processes that could contribute to the observed orientational dynamics. Anisotropy measurements report the orientational correlation function of a transition dipole moment vector. In the simplest scenario, anisotropy decay is a measure of molecular tumbling. Since the carbonyl stretch provides a more localized dipole moment, the anisotropy decay of the carbonyl stretch bleach in the deuterated isotopologue of (CH₃, CH₃) was measured. A much slower anisotropy decay time scale of ~20 ps was obtained (Figure S7), which is consistent with molecular reorientation time scales of relatively small molecules. ^{14,46–51} The anisotropy time scales measured in the OH and OD stretch regions, therefore, are too short for overall molecular reorientation.

Orientational relaxation could also arise from intermolecular vibrational energy transfer via the solvent to initially unexcited molecules. The slow recovery of the OH/OD stretch ground-state bleaches suggests that solute—solvent interactions are quite weak. Further, the anisotropy time scales measured here are longer than those reported in our previous study where CCl_4 was used as the solvent. If an intermolecular energy transfer mechanism were at play, we would expect faster

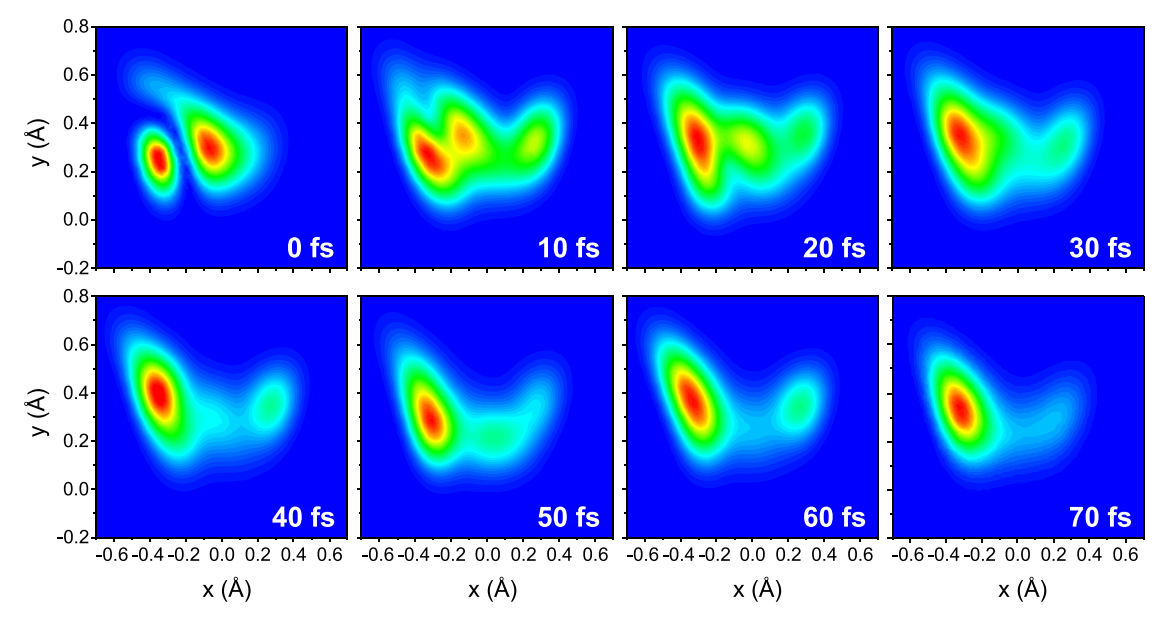


Figure 5. Evolution of the initially prepared probability P(x, y) for excitation of the OH stretch Ψ_3 state (CH₃, CH₃) and no initial excitation in normal modes (see eq 7). The H atom undergoes rapid dislocation between the donor and acceptor O atoms before relaxing back to the donor site.

orientational dynamics in the current measurements due to the more strongly interacting $CHCl_3/CDCl_3$ solvent. Instead, interactions with $CHCl_3/CDCl_3$ impede orientational relaxation, as expected when stronger solute—solvent interactions are present. We, therefore, rule out contributions from intermolecular energy transfer to the observed orientational dynamics.

Internal fluctuations, such as H atom rattling, can also contribute to anisotropy decay. To better understand the short-time dynamics following vibrational excitation, the probability evolution of the H atom OH stretch eigenstate $(\Psi_3$ in Figure 2b) was calculated using the procedures discussed above. The results are presented in Figure 5, while those for the deuterated isotopologue are provided in Figure S8. The H atom quickly becomes dislocated across the O-O axis within the first 10-20 fs following excitation, with significant probability predicted at the acceptor site. The H atom then rapidly relaxes back to the donor site, with small probability persisting at the acceptor oxygen atom. The D atom, meanwhile, is predicted to have more localized behavior. Fast, reversible dislocation of the H atom along the O-O axis, however, should not completely scramble the OH stretch dipole orientation. Small fluctuations of the H/D atoms around the equilibrium position⁵² should likewise result in partial anisotropy decay. 53,54 While rapid fluctuations of the H/D atom positions certainly contribute to the early time orientational dynamics, they should not contribute to the longer time scales nor result in complete decay of the anisotropy.

Intramolecular energy relaxation is also likely to contribute to the orientational dynamics given the significant mode coupling predicted by the time-independent calculations (Figure 3b,d). Figure 6a shows the short-time evolution of the energies for the 16 normal modes included in the calculations following excitation of the Ψ_3 state. The normal modes show an instantaneous response to OH excitation, corroborating the strong coupling predicted using the time-independent model. The strongest responses come from the key O–O motion (mode 5 in Figure 6a), several modes

involving motions of the methyl groups, and the out-of-plane (z-axis) motion of the H atom. Displacement vectors of the 16 normal modes are provided in Figure S9. Further, the complex evolution of the H atom wave function depicted in Figure 5 suggests coupling between the Ψ_n states. Figure 6b shows the probability evolution of H atom Ψ_n states following OH stretch excitation. The strong responses of the other zeroth-order states indicate significant mixing of the Ψ_n states in a time-independent picture. In particular, there are strong responses from the Ψ_1 ground state, Ψ_2 OH bend fundamental, and Ψ_5 OH stretch overtone. The complicated degree of mode mixing present likely contributes to the relatively low initial anisotropy values at time zero.

The total energy flow between the H atom $\{x, y\}$ and normal mode degrees of freedom is shown in Figure 6c. Energy within the normal mode coordinates plateaus in <100 fs. Similarly strong mode coupling and fast energy flow are predicted for the deuterated isotopologue (Figure S10). Given the lack of initial D atom dislocation, the 250 fs anisotropy component for deuterated (CH₃, CH₃), therefore, is attributed mainly to intramolecular vibrational energy relaxation out of the D atom degrees of freedom into the normal mode coordinates as well as relaxation of the OD stretch into the bending coordinate. Since the sub-100 fs component for the OH stretch occurs within the pulse overlap and window response region, it cannot be easily interpreted. Nevertheless, the similar relaxation dynamics measured and predicted between the two isotopologues suggests that the rapid initial dislocation of the H atom is a key contributor to the underlying fast anisotropy component of the light isotopologue.

The sizable isotopic difference observed in the long-time anisotropy components in (CH₃, CH₃) suggests that these time scales could correspond to orientational dynamics associated with the H/D atom transfer coordinate. The \sim 2 ps time scale measured for the OD stretch is consistent with the \sim 2 ps tunneling half-period predicted by Qu et al., ¹² while the \sim 600 fs time scale measured for the OH stretch is slightly slower than the predicted \sim 400 fs half-period ¹² but in-line with the classical H atom residence times (<700 fs) predicted by

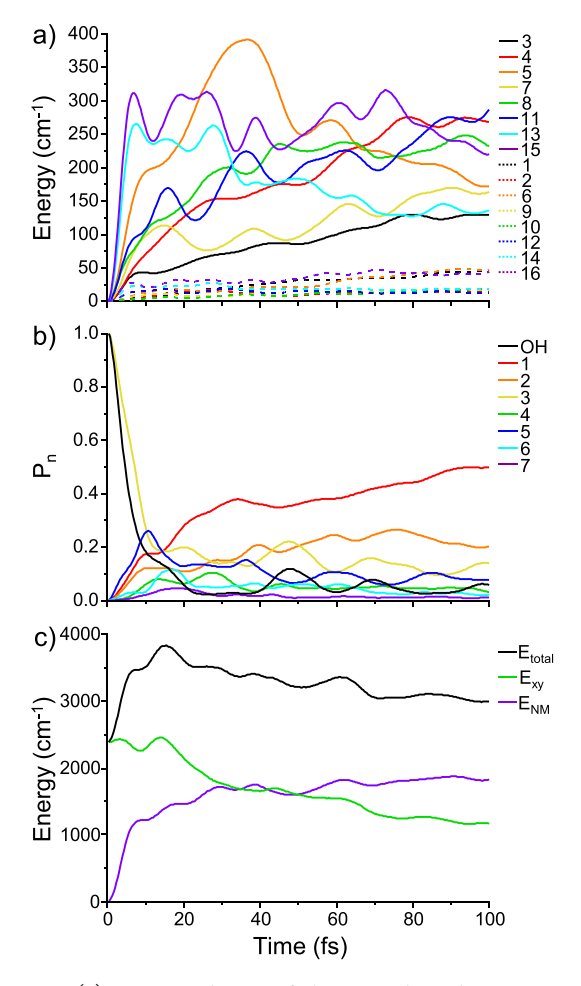


Figure 6. (a) Time evolution of the normal mode energies after excitation of the OH stretch Ψ_3 state. Mode 5 corresponds to the O–O motion. (b) Probability flow of the H atom $\{x, y\}$ eigenstates Ψ_n following excitation of the OH stretch. $P_{\rm OH}$ is the probability of being in the initial state. The remaining probabilities are the diagonal elements of the density matrix $P_n = d_{n,n}$ (see eq 7). (c) Total energies in the H atom $\{x, y\}$ (green) and normal mode degrees of freedom (purple), and the sum of the two (black).

Kaser et al.¹¹ It is interesting to note that the long-time anisotropy components occur well beyond the vibrational population relaxation dynamics. The displacement vectors for many of the coupled normal modes (Figure S9) occur roughly parallel to the O–O axis. The intramolecular motions induced by vibrational relaxation, therefore, are able to retain partial orientational memory of the initial excitation.

The 600 and 2000 fs time constants measured in the light and deuterated isotopologues correspond to \sim 4 and \sim 14 periods of the critical O–O motion, respectively. The loss of orientational memory over so many periods within vibrationally excited (CH₃, CH₃) infers that H/D atom transfer occurs through an activated process that involves additional molecular coordinates. The most prominent structural change between the C_s minimum and C_{2v} transition-state structures is rotation of the R₂ methyl group (Figure 1). To evaluate the influence of this methyl group on the H atom dynamics, we performed calculations with the R₂ methyl group rotated 60° to its transition-state configuration while keeping all other atoms held fixed at their equilibrium C_s positions (Figure 7a). The resulting H atom $\{x, y\}$ potential has a noticeably deeper well at the acceptor oxygen atom site (Figure 7b). The OH stretch

wave function is also significantly more delocalized across the transfer coordinate. Importantly, the calculated dynamics shows large amplitude motions of the H atom between the donor and acceptor sites that persist beyond 150 fs (Figure 7c). The results indicate that larger internal structural changes, including methyl end group rotations and changes in the CO and CC bond lengths, are required in addition to O–O motion to promote H/D atom transfer by stabilizing the product configuration. We hypothesize that orientational memory is irreversibly lost upon these collective internal structural rearrangements that enable a complete H/D atom transfer event.

(*Ph, Ph*). To see how the orientational dynamics respond to substitution of the (R_1, R_2) end groups, we begin with (Ph, Ph)Ph), the most strongly H-bonded species investigated. The H atom $\{x, y\}$ potential is very shallow, with the zero-point level falling only 1000 cm⁻¹ below the barrier in the frozen molecule. As a result, the OH and OD stretch eigenstates lie above the barrier leading to highly delocalized wave functions (Figure 8a,b) that exhibit strong bend-stretch mixing. The 2D IR spectra once again reveal very broad ground-state bleach OH/OD stretch features in both isotopologues (Figure 8c,d) that are slightly lower in energy compared to (CH₃, CH₃). The substructure in the OD stretch region results from weak absorptions that appear in the linear infrared spectrum and derive from the phenyl groups, presumably from overtone and/or combination bands.⁵⁵ The TA spectra for (Ph, Ph) are provided in Figure S11.

The anisotropy decay dynamics for (Ph, Ph) are presented in Figure 8e,f for the OH and OD stretch regions, respectively. Interestingly, a single exponential decay component with a time constant of ~200 fs is obtained in both isotopologues. A recent computational study by Etinski and Ensing on (Ph, Ph) predicted a very low H atom transfer barrier height of <300 cm⁻¹, with the zero-point level just slightly below the barrier. So The ground-state wave function of the H atom was predicted to be delocalized across the transfer coordinate with an average position at the transfer midpoint. Room temperature simulations also predicted a large probability distribution in the O-O distance spanning 2.4-2.6 Å. The computational predictions point to a scenario in which the H atom is highly delocalized between the donor and acceptor sites in the ground state at room temperature. This inherent delocalization could account for the lack of a very fast initial anisotropy component in the light isotopologue. The nearly identical time scales between light and deuterated (Ph, Ph) imply that the D atom is also delocalized in the ground state.

Our calculations predict the two phenyl groups to have a small dihedral twist of $\sim 13^{\circ}$ with respect to the carbon atom backbone. The planar C_s conformer, however, is predicted to be isoenergetic. The small torsional angles and barriers of the phenyl groups mean that large internal structural rearrangements will not be present in (Ph, Ph) and are not required to promote H/D transfer. Consequently, the orientational relaxation dynamics are expected to be governed by intramolecular vibrational energy relaxation. This interpretation is consistent with the similar ~ 200 fs anisotropy decay time scales for both (Ph, Ph) isotopologues and deuterated (CH₃, CH₃).

(CH₃, Ph). The shallowness of the H atom $\{x, y\}$ potential for (CH₃, Ph) is intermediate to those of (Ph, Ph) and (CH₃, CH₃). While the OH stretch wave function is highly delocalized across the transfer coordinate (Figure 9a), the

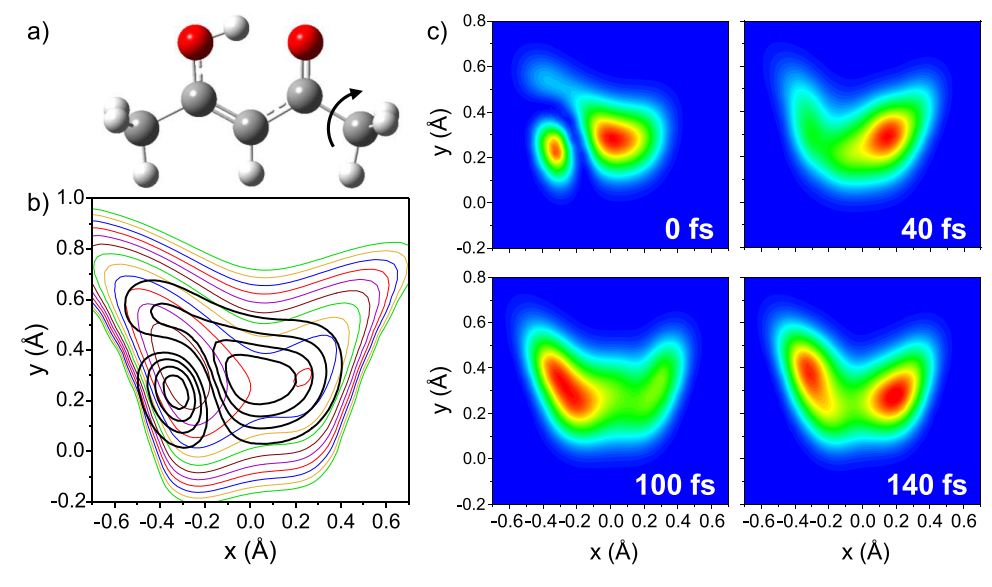


Figure 7. (a) Structure of (CH_3, CH_3) with the R_2 methyl group rotated to the transition-state orientation with all other atoms held fixed at the minimum-energy positions. (b) Corresponding H atom $\{x, y\}$ potential and OH stretch wave function demonstrating a lower barrier and increased dislocation between the donor and acceptor sites. (c) Probability evolution of the initially prepared OH stretch showing large amplitude motion of the H atom across the transfer coordinate. The basis set was $\{M, N, K\} = \{8, 14, 9\}$.

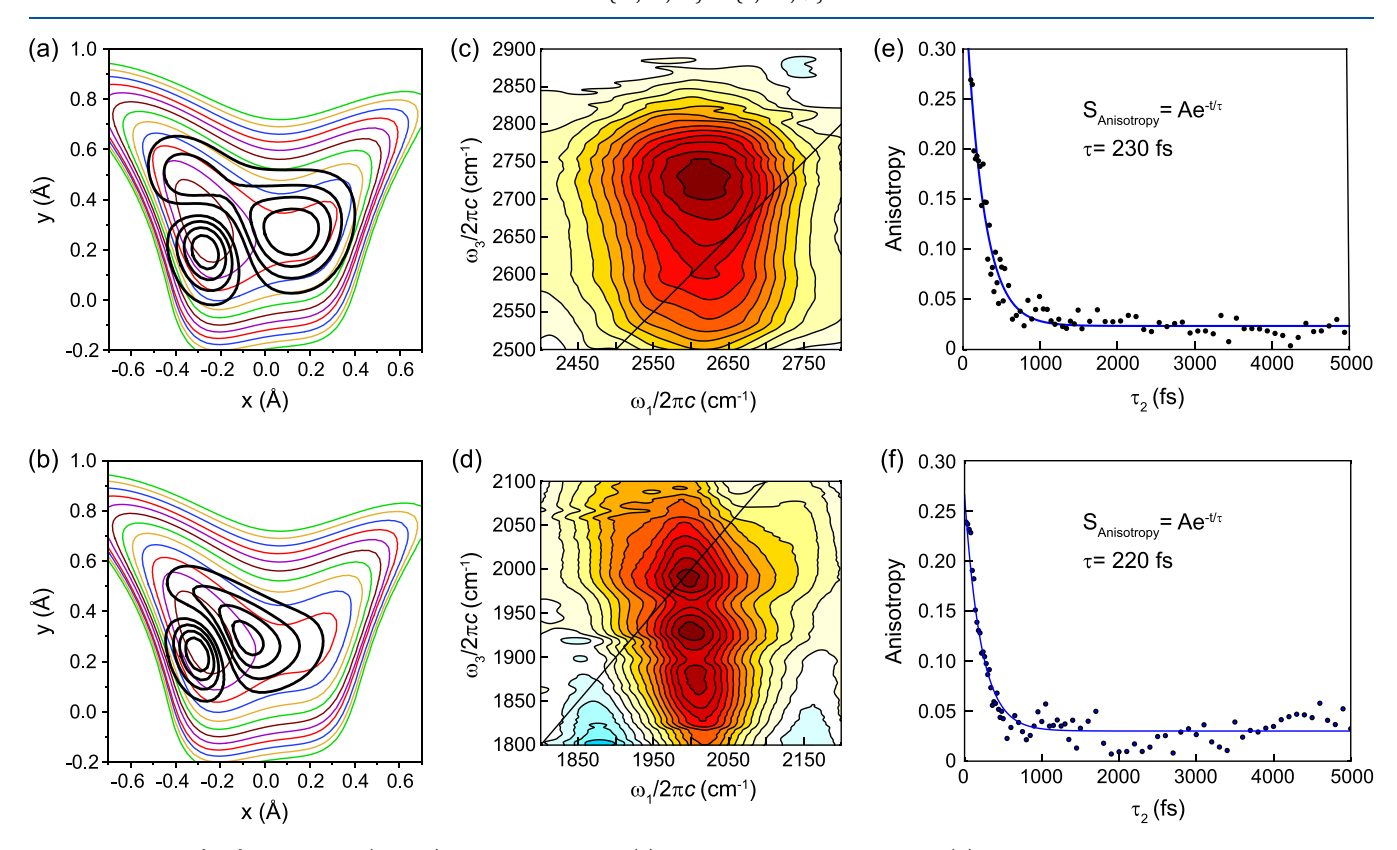


Figure 8. H atom $\{x, y\}$ potential of (Ph, Ph) superimposed with (a) OH stretch wave function and (b) OD stretch wave function. Isotropic 2D IR spectra collected at 150 fs waiting time for (c) (Ph, Ph) in the OH stretch region and (d) d_2 -(Ph, Ph) in the OD stretch region. Polarization anisotropy measurements for (e) (Ph, Ph) and (f) d_2 -(Ph, Ph). Both anisotropies were fit to monoexponential decays with time constants ~200 fs.

higher barrier in the frozen molecule results in a more localized OD stretch wave function compared to (Ph, Ph) (Figure 9b). The 2D IR spectra of (CH₃, Ph) are quite similar in appearance and breadth to (Ph, Ph) in both the OH stretch (Figure 9c) and OD stretch (Figure 9d) regions (the sharper diagonal elongation at lower pump frequencies in Figure 9c is derived from pump scatter). There is no spectral evidence of

two distinct bleach features corresponding to the two inequivalent minima. The TA spectra also do not exhibit any notable evolution of the bleach features (Figure S12). The higher-energy isomer with the H bound closest to the Ph group is predicted to have a similar O—O distance and OH stretch frequency to the global minimum. The low barrier to transfer likely results in initial populations of both isomers. The

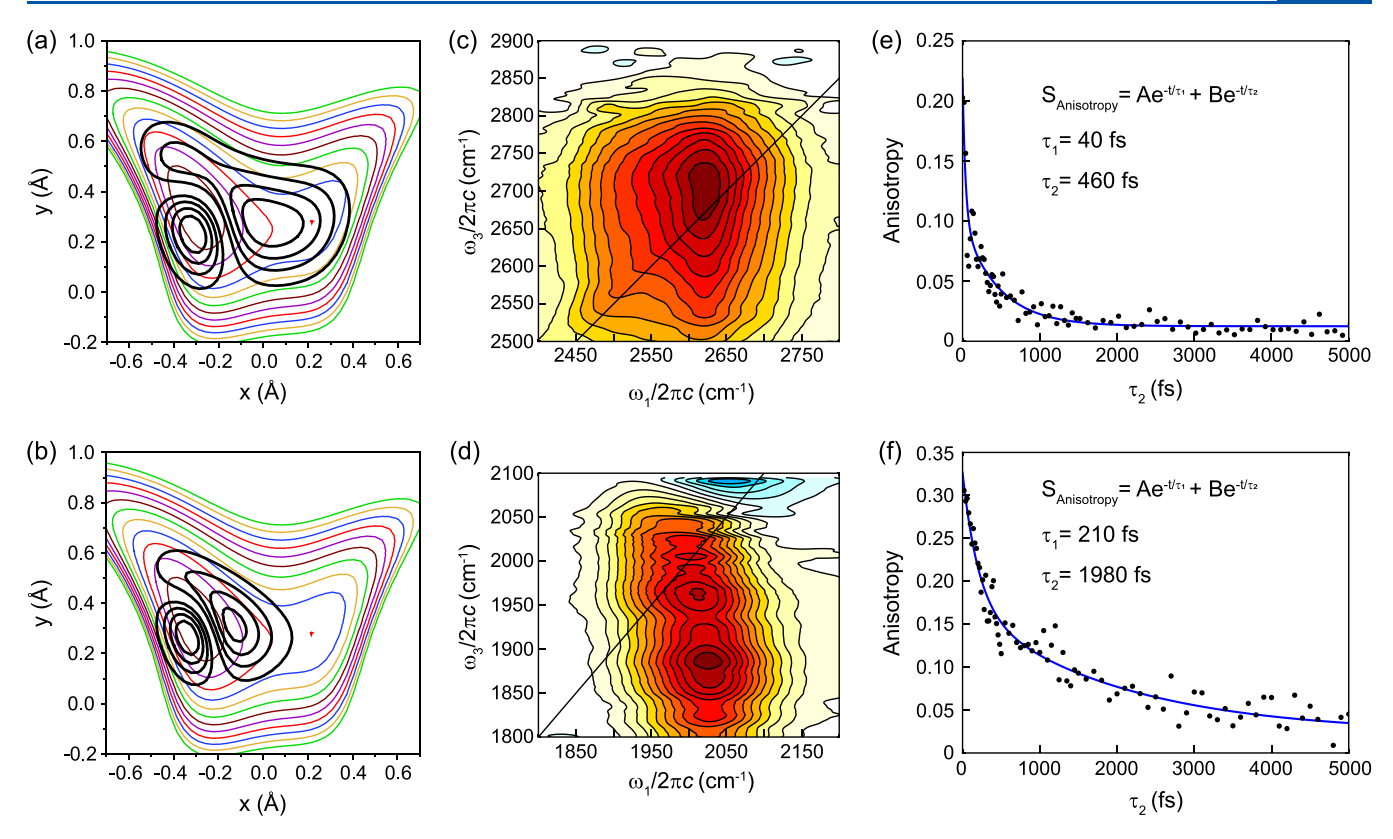


Figure 9. H atom $\{x, y\}$ potential of (CH₃, Ph) superimposed with (a) OH stretch wave function and (b) OD stretch wave function. Isotropic 2D IR spectra were collected at 150 fs waiting time for (c) (CH₃, Ph) in the OH stretch region and (d) d_2 -(CH₃, Ph) in the OD stretch region. Polarization anisotropy measurements for (e) (CH₃, Ph) and (f) d_2 -(CH₃, Ph). Both anisotropies were fit to biexponential decays with time constants presented in the figure and summarized in Table 2.

broad, overlapping spectral signatures from both isomers are likely spectroscopically indistinct.

The anisotropy decay of the OH stretch in (CH3, Ph) is presented in Figure 9e and is more similar to that of (CH₃, CH₃) than to that of (Ph, Ph). A very rapid initial decay is observed followed by a slower decay component of ~460 fs that is slightly faster but statistically similar to that in (CH₃, CH₃). The anisotropy decay of the OD stretch is also nearly identical to that in deuterated (CH₃, CH₃), with a \sim 200 fs fast component and a \sim 2000 fs slow component (Figure 9f). The close similarity between (CH₃, Ph) and (CH₃, CH₃) suggests common mechanisms driving orientational relaxation in these species. Although (CH₃, Ph) has a shorter O-O distance and stronger H-bond than (CH₃, CH₃), the asymmetry in the PES and barrier height are sufficient to yield a more localized ground-state H atom compared to (Ph, Ph). As a result, the H atom will undergo rapid dislocation upon vibrational excitation while the D atom will remain more localized, yielding fast anisotropy components similar to (CH3, CH3). Larger structural rearrangements, particularly rotation of the R₁ methyl group, are then necessary to promote H/D atom transfer. Torsional motion of the single Ph group should again negligibly contribute to the orientational relaxation dynamics. Interestingly, the calculations predict only a partial rotation of $\sim 32^{\circ}$ of the R₁ methyl group upon H/D transfer. These factors, along with the stronger H-bond interaction, might contribute to the slightly shorter long-time anisotropy components measured in (CH₃, Ph) compared to those in (CH₃, CH₃).

(CH₃, CF₃). We next turn to the fluorinated species, which are predicted to have weaker H-bonds. The H atom potential for (CH₃, CF₃) is presented in Figure 10. The barrier height (~5000 cm⁻¹) predicted for the frozen molecule is higher than those of the more strongly H-bonded species discussed above. The OH (Figure 10a) and OD (Figure 10b) stretch wave functions are also much more localized compared to the other species. The 2D IR spectrum in the OH stretch region (Figure 10c) exhibits a broad ground-state bleach signature centered near 3000 cm⁻¹. The 2D IR spectrum in the OD stretch region is given in Figure 10d and likewise exhibits a broad groundstate bleach feature. TA spectra are provided in Figure S13. The long-lived and broad bleach signals indicate that relatively strong coupling of the H and D degrees of freedom to the normal mode coordinates remains present in (CH₃, CF₃). Similar to the case for (CH₃, Ph), there is no evidence of distinct bleach signals from the two possible isomers. Larger structural differences are predicted for the higher-energy isomer where the H resides on the acceptor site (toward CF₃), in particular, a contraction of the O-O distance by ~0.03 Å. Harmonic calculations predict a red-shift of >100 cm⁻¹ for the OH stretch of the high-energy isomer. The OH stretch signature for this isomer could either fall below the pulse bandwidth, overlap with the measured bleach, or be too weak due to a low population.

The anisotropy decay dynamics, interestingly, are consistent with those of (CH_3, CH_3) and (CH_3, Ph) despite the weaker H-bond. The OH stretch anisotropy (Figure 10e) exhibits a fast initial decay, followed by a slower decay component with a \sim 600 fs time constant. The anisotropy decay dynamics in the

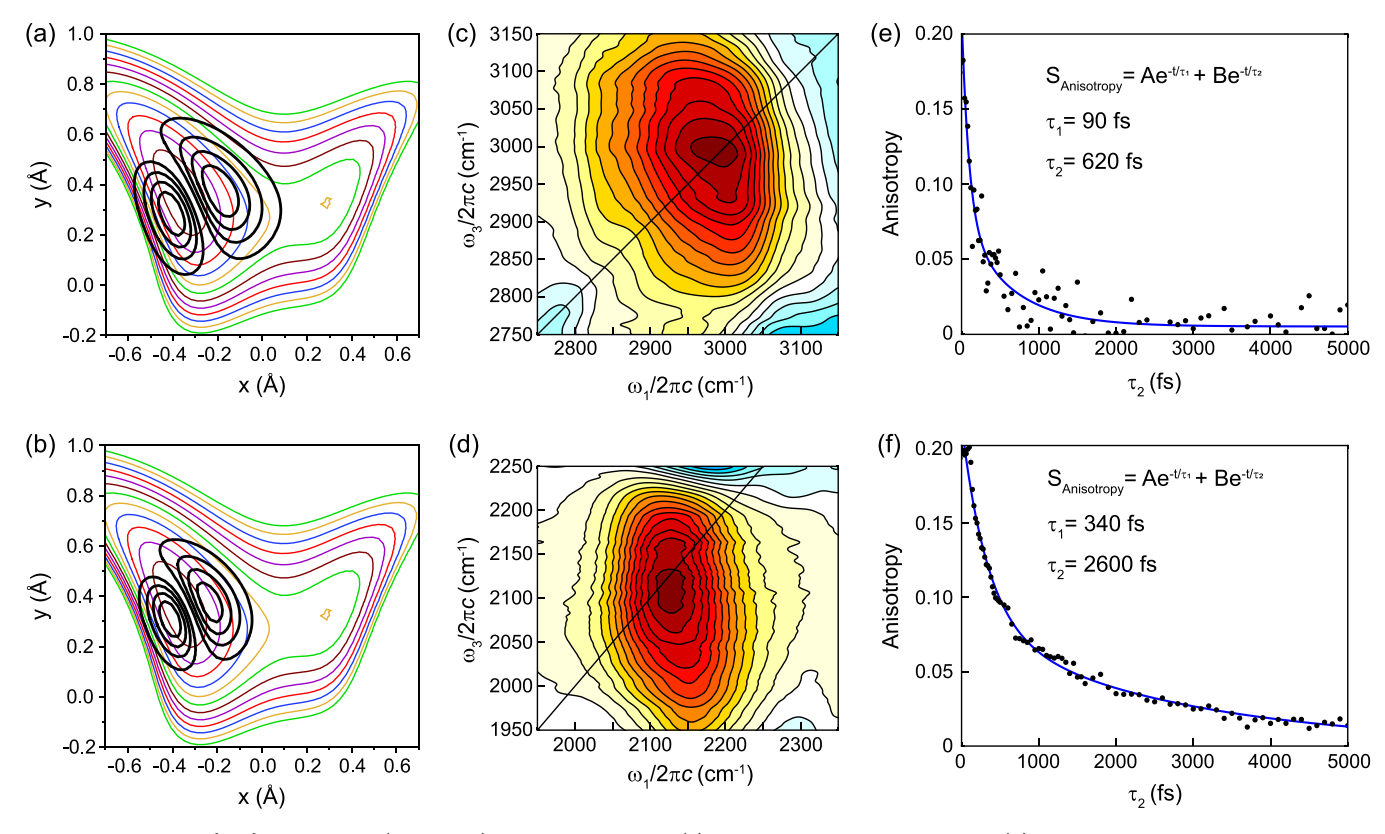


Figure 10. H atom $\{x, y\}$ potential of (CH_3, CF_3) superimposed with (a) OH stretch wave function and (b) OD stretch wave function. Isotropic 2D IR spectra collected at a 150 fs waiting time for (c) (CH_3, CF_3) in the OH stretch region and (d) d_2 - (CH_3, CF_3) in the OD stretch region. Polarization anisotropy measurements for (e) (CH_3, CF_3) and (f) d_2 - (CH_3, CF_3) . Both anisotropies were fit to biexponential decays with time constants presented in the figure and summarized in Table 2.

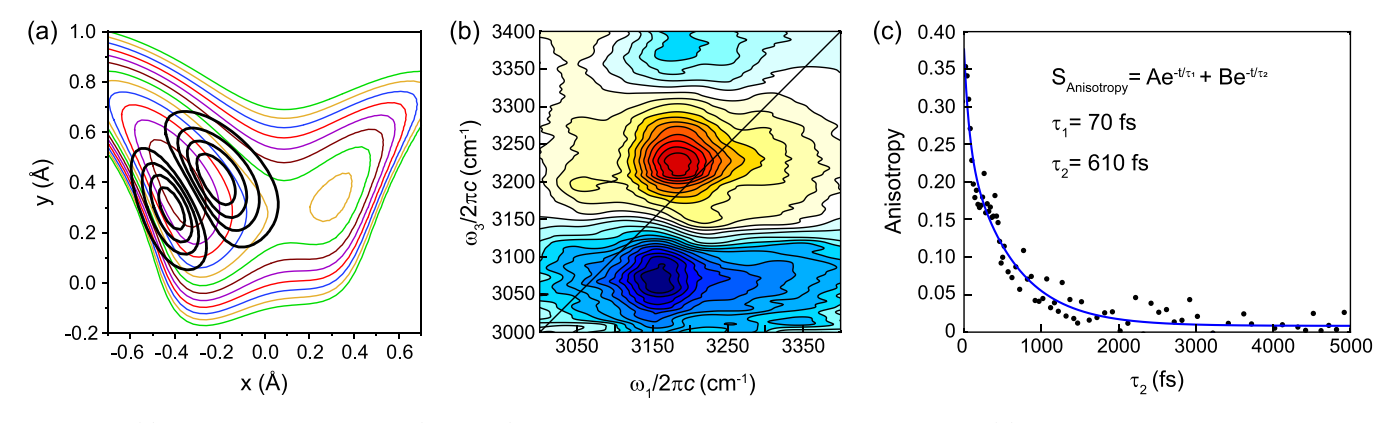


Figure 11. (a) H atom $\{x, y\}$ potential of (CF_3, CF_3) superimposed with the OH stretch wave function. (b) Isotropic 2D IR spectrum collected at 150 fs in the OH stretch region. A strong induced absorption feature consistent with an overtone transition is observed. (c) Polarization anisotropy measurements in the OH stretch region. The anisotropy was fit to a biexponential decay with time constants presented in the figure and summarized in Table 2.

OD stretch region (Figure 10f) are slightly slower compared to those of the other species, with a $\sim\!\!300$ fs fast component and a $\sim\!\!2600$ fs slow component. The slower orientational dynamics likely reflect the weaker H-bond interaction in (CH $_3$, CF $_3$) and the more localized D atom. The overall similarity of the anisotropy dynamics again infers a common orientational relaxation mechanism that involves activated, collective internal motions.

(CF₃, CF₃). The H atom potential for (CF₃, CF₃), the species with the weakest H-bond, is presented in Figure 11a. The potential has the largest barrier (\sim 5500 cm⁻¹) between the donor and acceptor sites. Consequently, the OH stretch

wave function is calculated to be the most localized among the studied species and shows the least amount of bend character. The 2D IR spectrum in the OH stretch region is presented in Figure 11b. A relatively strong induced absorption feature appears ~200 cm⁻¹ lower in energy than the ground-state bleach. This feature is consistent with an induced overtone transition typically observed in 2D IR spectra. The induced absorption decays rapidly with a time constant of <100 fs to a constant induced absorption background signal (Figure S14). The rapid vibrational lifetime decay dynamics indicates that excitation energy in the OH stretch relaxes quickly despite the weaker H-bond and more localized wave function. Although

Table 2. Time Constants and Normalized Amplitudes of the Biexponential Decay Fits to the Anisotropy Measurements^a

	OH stretch				OD stretch			
Species	$ au_1/ ext{fs}$	A_1	$ au_2/ ext{fs}$	A_2	$ au_1/ ext{fs}$	\mathbf{A}_1	$ au_2/ ext{fs}$	A_2
(Ph, Ph)	220(10)	1	-	-	210(10)	1	-	-
(CH ₃ , Ph)	40(10)	0.57(7)	460(80)	0.42(5)	210(40)	0.51(6)	1980(380)	0.49(6)
(CH_3, CH_3)	50(10)	0.85(9)	650(140)	0.15(2)	240(20)	0.61(3)	2160(290)	0.39(3)
(CH ₃ , CF ₃)	90(30)	0.66(10)	620(200)	0.34(10)	340(20)	0.61(3)	2600(390)	0.39(1)
(CF ₃ , CF ₃)	70(20)	0.33(7)	610(70)	0.67(6)	-	-	-	-

^a(Ph, Ph) was fit to a monoexponential decay. Numbers in parentheses are the standard deviations in the fit parameters to the indicated digits.

the degree of anharmonic coupling to low-frequency modes will be less in (CF₃, CF₃) than that predicted for (CH₃, CH₃), they are still significant enough to induce fast relaxation dynamics. A persistent induced absorption signal also appears at higher energy along the probe axis. The appearance of long-lived induced absorption signals at both lower and higher energies to the ground-state bleach indicates an overall broadening of the OH stretch manifold within the hot molecule following intramolecular vibrational relaxation. ^{57–62}

The anisotropy dynamics for (CF₃, CF₃) in the OH stretch region are presented in Figure 11c (the hydrolysis reaction of (CF₃, CF₃) prevented the synthesis of the deuterated isotopologue). The anisotropy begins close to the expected value of 0.4, another indication of the weaker mode coupling and greater localization of the H atom in (CF₃, CF₃). The anisotropy decay time constants, however, are once again quite similar to those of the other β -diketones. Following an initial rapid component, the anisotropy decays with a slow component of ~600 fs. In contrast to the other species, the slower time scale is the dominant decay component with an amplitude of ~ 0.7 . Given the lesser degree of mode coupling and dislocation, the structural rearrangements that accompany H atom transfer appear to be the main contributor to the anisotropy decay dynamics in vibrationally excited (CF₃, CF₃). The anisotropy decay dynamics for each species are summarized in Table 2.

CONCLUSIONS

The vibrational spectral signatures of the strong intramolecular H-bond in a series of β -diketones were investigated by using ultrafast infrared spectroscopies and computational modeling that accounts for coupling of the H atom degrees of freedom to the other normal mode coordinates. In general, the H atom potentials are predicted to be very soft, with low-energy pathways between the H atom donor and acceptor sites. The soft potentials result in strong anharmonic coupling between the H atom degrees of freedom and many normal mode coordinates. This coupling gives rise to the very broad and relatively weak OH stretch absorption features measured experimentally. In a time-dependent picture, the H atom becomes rapidly dislocated upon vibrational excitation and quickly returns to the ground state as energy relaxes into the coupled normal mode vibrations. The 2D IR spectral signatures manifest as homogeneously broadened OH stretch ground-state bleaches of the vibrationally hot molecules. Induced overtone transitions were not observed for the most strongly H-bonded species and are predicted to fall much lower in energy due to the significant anharmonicity of the soft H atom potentials. The exception was (CF₃, CF₃), which exhibited a short-lived, highly red-shifted induced absorption transition. Meanwhile, the D atoms in the heavier isotopologues are predicted to be more localized upon vibrational excitation. The soft potentials, however, still yield significant coupling between the D atom degrees of freedom and the other normal mode coordinates. Experimentally, TA and 2D IR spectra in the OD stretch regions show characteristics similar to those of the OH stretches.

Polarization-sensitive TA measurements were utilized to probe the orientational relaxation dynamics. Surprisingly longlived and isotope-dependent anisotropy decays were measured and are attributed to activated, collective internal structural rearrangements that are required for successful intramolecular H/D atom transfer events. Recent computational analyses on intramolecular H atom transfer in the model system 6-hydroxy-2-formylfulvene reached similar conclusions.⁶³ This interpretation is also very similar to that provided for the aqueous proton, 64 where long-lived polarization anisotropy was ascribed to concerted reorganization of the local H-bond network that accompanies irreversible proton transfer. 65-68 Analogous to intermolecular reorganization in water, intramolecular structural rearrangements in β -diketones appear to be necessary to promote and stabilize the formation of the H atom transfer product, after which the system loses orientational memory of the initial configuration. Despite the differences in H-bond strengths and H atom donor-acceptor distances, the orientational relaxation time scales are remarkably conserved with common relaxation time scales of ~600 and ~2000 fs for the light and heavy isotopologues, respectively. The one exception is (Ph, Ph), where both isotopologues display fast 200 fs anisotropy decays, consistent with inherently delocalized H and D atoms in the ground state. While the measured time scales are consistent with computational predictions for intramolecular H/D atom transfer dynamics within strongly H-bonded β -diketones in the vibrational ground state, ^{4,11,12,56} the measured dynamics reported here were made on vibrationally hot molecules. With significant coupling and relaxation into many low-frequency modes, including the crucial O-O mode, the inferred transfer time scales provide a lower limit for H/D atom transfer within the vibrational ground states.

ASSOCIATED CONTENT

Solution Supporting Information

The Supporting Information is available free of charge at https://pubs.acs.org/doi/10.1021/acs.jpca.3c05417.

Optimized calculated structures for the five systems; H atom $\{x, y\}$ wave functions for (CH_3, CH_3) ; D atom $\{x, y\}$ wave functions for (CH_3, CH_3) ; comparison of B3LYP and CCSD(T) H atom potential barriers; H atom potentials and wave functions using the CCSD(T) potential of Qu et al.; isotropic ground-state bleach dynamics; anisotropy decay dynamics for the carbonyl

stretch of deuterated (CH₃, CH₃); short-time D atom dynamics for vibrationally excited (CH₃, CH₃); normal mode displacement vectors for the 16 coupled modes in (CH₃, CH₃); normal mode response and energy flow dynamics in deuterated (CH₃, CH₃); TA spectra of (Ph, Ph); TA spectra of (CH₃, Ph); TA spectra of (CH₃, CF₃); TA spectra of (CF₃, CF₃); and computational details involving methyl group rotation (PDF)

AUTHOR INFORMATION

Corresponding Authors

Edwin L. Sibert III – Department of Chemistry and Theoretical Chemistry Institute, University of Wisconsin Madison, Madison, Wisconsin 53706, United States; orcid.org/0000-0003-2752-1044; Email: elsibert@wisc.edu

Joseph A. Fournier — Department of Chemistry, Washington University in St. Louis, St. Louis, Missouri 63130, United States; orcid.org/0000-0001-7569-9176; Email: jfournier@wustl.edu

Authors

Jessika L.S. Dean – Department of Chemistry, Washington University in St. Louis, St. Louis, Missouri 63130, United States

Valerie S. Winkler – Department of Chemistry, Washington University in St. Louis, St. Louis, Missouri 63130, United States

Mark A. Boyer – Department of Chemistry and Theoretical Chemistry Institute, University of Wisconsin Madison, Madison, Wisconsin 53706, United States

Complete contact information is available at: https://pubs.acs.org/10.1021/acs.jpca.3c05417

Author Contributions

§J.L.S.D. and V.S.W. contributed equally.

Notes

The authors declare no competing financial interest.

■ ACKNOWLEDGMENTS

E.L.S. gratefully acknowledges support from the National Science Foundation (NSF) via Grant CHE-1900095. J.A.F. acknowledges support from NSF through a CAREER Award (Grant CHE-2044927).

■ REFERENCES

- (1) Baba, T.; Tanaka, T.; Morino, I.; Yamada, K. M. T.; Tanaka, K. Detection of the Tunneling-Rotation Transitions of Malonaldehyde in the Submillimeter-Wave Region. *J. Chem. Phys.* **1999**, *110* (9), 4131–4133.
- (2) Terranova, Z. L.; Corcelli, S. A. Monitoring Intramolecular Proton Transfer with Two-Dimensional Infrared Spectroscopy: A Computational Prediction. *J. Phys. Chem. Lett.* **2012**, 3 (13), 1842–1846.
- (3) Dannenberg, J. J.; Rios, R. Theoretical Study of the Enolic Forms of Acetylacetone How Strong Is the H-Bond? *J. Phys. Chem.* **1994**, 98 (27), 6714–6718.
- (4) Qu, C.; Conte, R.; Houston, P. L.; Bowman, J. M. Full-Dimensional Potential Energy Surface for Acetylacetone and Tunneling Splittings. *Phys. Chem. Chem. Phys.* **2021**, 23 (13), 7758–7767.
- (5) Mavri, J.; Grdadolnik, J. Proton Potential in Acetylacetone. J. Phys. Chem. A 2001, 105 (10), 2039–2044.

- (6) Caminati, W.; Grabow, J. U. The C_{2v} Structure of Enolic Acetylacetone. J. Am. Chem. Soc. **2006**, 128 (3), 854–857.
- (7) Tayyari, S. F.; Milani-nejad, F. Vibrational Assignment of Acetylacetone. Spectrochim. Acta, Part A 2000, 56 (14), 2679–2691.
- (8) Matanovic, I.; Doslic, N.; Mihalic, Z. Exploring the Potential Energy Surface for Proton Transfer in Acetylacetone. *Chem. Phys.* **2004**, 306 (1–3), 201–207.
- (9) Broadbent, S. A.; Burns, L. A.; Chatterjee, C.; Vaccaro, P. H. Investigation of Electronic Structure and Proton Transfer in Ground State Acetylacetone. *Chem. Phys. Lett.* **2007**, 434 (1–3), 31–37.
- (10) Howard, D. L.; Kjaergaard, H. G.; Huang, J.; Meuwly, M. Infrared and Near-Infrared Spectroscopy of Acetylacetone and Hexafluoroacetylacetone. *J. Phys. Chem. A* **2015**, *119* (29), 7980–7990
- (11) Kaser, S.; Unke, O. T.; Meuwly, M. Reactive Dynamics and Spectroscopy of Hydrogen Transfer from Neural Network-Based Reactive Potential Energy Surfaces. *New J. Phys.* **2020**, 22 (5), 18.
- (12) Qu, C.; Houston, P. L.; Conte, R.; Nandi, A.; Bowman, J. M. Breaking the Coupled Cluster Barrier for Machine-Learned Potentials of Large Molecules: The Case of 15-Atom Acetylacetone. *J. Phys. Chem. Lett.* **2021**, *12* (20), 4902–4909.
- (13) Stenger, J.; Madsen, D.; Dreyer, J.; Hamm, P.; Nibbering, E. T. J.; Elsaesser, T. Femtosecond Mid-Infrared Photon Echo Study of an Intramolecular Hydrogen Bond. *Chem. Phys. Lett.* **2002**, 354 (3–4), 256–263.
- (14) Madsen, D.; Stenger, J.; Dreyer, J.; Hamm, P.; Nibbering, E. T. J.; Elsaesser, T. Femtosecond Mid-Infrared Pump-Probe Study of Wave Packet Motion in a Medium-Strong Intramolecular Hydrogen Bond. *Bull. Chem. Soc. Jpn.* **2002**, *75* (5), 909–917.
- (15) Stenger, J.; Madsen, D.; Dreyer, J.; Nibbering, E. T. J.; Hamm, P.; Elsaesser, T. Coherent Response of Hydrogen Bonds in Liquids Probed by Ultrafast Vibrational Spectroscopy. *J. Phys. Chem. A* **2001**, 105 (13), 2929–2932.
- (16) Heyne, K.; Huse, N.; Nibbering, E. T. J.; Elsaesser, T. Coherent Vibrational Dynamics of Intermolecular Hydrogen Bonds in Acetic Acid Dimers Studied by Ultrafast Mid-Infrared Spectroscopy. *J. Phys.: Condens. Matter* **2003**, *15* (1), S129–S136.
- (17) Heyne, K.; Huse, N.; Nibbering, E. T. J.; Elsaesser, T. Ultrafast Coherent Nuclear Motions of Hydrogen Bonded Carboxylic Acid Dimers. *Chem. Phys. Lett.* **2003**, *369* (5–6), 591–596.
- (18) Heyne, K.; Huse, N.; Nibbering, E. T. J.; Elsaesser, T. Ultrafast Relaxation and Anharmonic Coupling of O-H Stretching and Bending Excitations in Cyclic Acetic Acid Dimers. *Chem. Phys. Lett.* **2003**, 382 (1–2), 19–25.
- (19) Petersen, P. B.; Roberts, S. T.; Ramasesha, K.; Nocera, D. G.; Tokmakoff, A. Ultrafast N-H Vibrational Dynamics of Cyclic Doubly Hydrogen-Bonded Homo- and Heterodimers. *J. Phys. Chem. B* **2008**, *112* (42), 13167–13171.
- (20) Van Hoozen, B. L.; Petersen, P. B. Origin of the 900 cm⁻¹ Broad Double-Hump OH Vibrational Feature of Strongly Hydrogen-Bonded Carboxylic Acids. *J. Chem. Phys.* **2015**, *142*, 104308.
- (21) Van Hoozen, B. L.; Petersen, P. B. A Combined Electronic Structure and Molecular Dynamics Approach to Computing the OH Vibrational Feature of Strongly Hydrogen-Bonded Carboxylic Acids. *J. Chem. Phys.* **2017**, *147* (22), 224304.
- (22) Stingel, A. M.; Petersen, P. B. Couplings Across the Vibrational Spectrum Caused by Strong Hydrogen Bonds: A Continuum 2D IR Study of the 7-Azaindole-Acetic Acid Heterodimer. *J. Phys. Chem. B* **2016**, 120 (41), 10768–10779.
- (23) Heyne, K.; Huse, N.; Dreyer, J.; Nibbering, E. T. J.; Elsaesser, T.; Mukamel, S. Coherent Low-Frequency Motions of Hydrogen Bonded Acetic Acid Dimers in the Liquid Phase. *J. Chem. Phys.* **2004**, *121* (2), 902–913.
- (24) Costard, R.; Greve, C.; Fidder, H.; Nibbering, E. T. J. Hydrogen Bonding Induced Enhancement of Fermi Resonances: Ultrafast Vibrational Energy Flow Dynamics in Aniline-d5. *J. Phys. Chem. B* **2015**, *119* (6), 2711–2725.
- (25) Dahms, F.; Fingerhut, B. P.; Nibbering, E. T. J.; Pines, E.; Elsaesser, T. Large-Amplitude Transfer Motion of Hydrated Excess

- Protons Mapped by Ultrafast 2D IR Spectroscopy. *Science* **2017**, 357, 491–495.
- (26) Fournier, J. A.; Carpenter, W. B.; Lewis, N. H. C.; Tokmakoff, A. Broadband 2D IR Spectroscopy Reveals Dominant Asymmetric $H_5O_2^+$ Proton Hydration Structures in Acid Solutions. *Nat. Chem.* **2018**, *10* (9), 932–937.
- (27) Yu, Q.; Bowman, J. M. High-Level Quantum Calculations of the IR Spectra of the Eigen, Zundel, and Ring Isomers of $H^+(H_2O)_4$ Find a Single Match to Experiment. *J. Am. Chem. Soc.* **2017**, 139 (32), 10984–10987.
- (28) Carpenter, W. B.; Yu, Q.; Hack, J. H.; Dereka, B.; Bowman, J. M.; Tokmakoff, A. Decoding the 2D IR Spectrum of the Aqueous Proton with High-Level VSCF/VCI Calculations. *J. Chem. Phys.* **2020**, 153 (12), 17.
- (29) Dereka, B.; Yu, Q.; Lewis, N. H. C.; Carpenter, W. B.; Bowman, J. M.; Tokmakoff, A. Crossover from Hydrogen to Chemical Bonding. *Science* **2021**, *371* (6525), 160–164.
- (30) Dean, J. L. S.; Fournier, J. A. Vibrational Dynamics of the Intramolecular H-Bond in Acetylacetone Investigated with Transient and 2D IR Spectroscopy. *J. Phys. Chem. B* **2022**, *126* (19), 3551–3562.
- (31) Kaindl, R. A.; Wurm, M.; Reimann, K.; Hamm, P.; Weiner, A. M.; Woerner, M. Generation, Shaping, and Characterization of Intense Femtosecond Pulses Tunable from 3 to 20 μ m. *J. Opt. Soc. Am. B* **2000**, *17*, 2086–2094.
- (32) Shim, S.-H.; Zanni, T.; M. How to Turn Your Pump-Probe Instrument into a Multidimensional Spectrometer: 2D IR and Vis Spectroscopies via Pulse Shaping. *Phys. Chem. Chem. Phys.* **2009**, *11* (5), 748-761.
- (33) Blodgett, K. N.; Fischer, J. L.; Zwier, T. S.; Sibert, E. L. The Missing NH Stretch Fundamental in S₁ Methyl Anthranilate: IR-UV Double Resonance Experiments and Local Mode Theory. *Phys. Chem. Chem. Phys.* **2020**, 22, 14077–14087.
- (34) Sibert, E. L. I.; Blodgett, K. N.; Zwier, T. S. Spectroscopic Manifestations of Indirect Vibrational State Mixing: Novel Anharmonic Effects on a Prereactive H Atom Transfer Surface. *J. Phys. Chem. A* **2021**, *125* (33), 7318–7330.
- (35) Carrington, T.; Miller, W. H. Reaction Surface Description of Intramolecular Hydrogen Atom Transfer in Malonaldehyde. *J. Chem. Phys.* **1986**, 84 (8), 4364–4370.
- (36) Barnes, G. L.; Sibert, E. L., III. The Effects of Asymmetric Motions on the Tunneling Splittings in Formic Acid Dimer. *J. Chem. Phys.* **2008**, *129* (16), 164317.
- (37) Wilson, E. B.; Decius, J. C.; Cross, P. C. Molecular Vibrations: The Theory of Infrared and Raman Vibrational Spectra; McGraw-Hill: New York, 1955.
- (38) Frisch, M. Ea; Trucks, G. W.; Schlegel, H. B.; Scuseria, G. E.; Robb, M. A.; Cheeseman, J. R.; Scalmani, G.; Barone, V.; Petersson, G. A.; Nakatsuji, H. *Gaussian 16, Revision C. 01*, 2016.
- (39) Colbert, D. T.; Miller, W. H. A Novel Discrete Variable Representation for Quantum Mechanical Reactive Scattering via the S-Matrix Kohn Method. *J. Chem. Phys.* **1992**, *96* (3), 1982.
- (40) Stanton, F.; J. On the Vibronic Level Structure in the NO₃ Radical: II. Adiabatic Calculation of the Infrared Spectrum. *Mol. Phys.* **2009**, *107* (8–12), 1059–1075.
- (41) Davidson, E. R. Methods in Computational Molecular Physics. In *NATO Advanced Study Institute, Series C*; Plenum New York, 1983; Vol. 113, p 95.
- (42) Cullum, J. K.; Willoughby, R. A. Lanczos Algorithms for Large Symmetric Eigenvalue Computations: Vol. I: Theory; Birkhäuser: Boston. 1985.
- (43) Askar, A.; Cakmak, A. S. Explicit Integration Method for the Time-dependent Schrodinger Equation for Collision Problems. *J. Chem. Phys.* **1978**, *68* (6), 2794–2798.
- (44) Chen, L.; Sibert, E. L. I.; Fournier, J. A. Unraveling the Vibrational Spectral Signatures of a Dislocated H Atom in Model Proton-Coupled Electron Transfer Dyad Systems. *J. Phys. Chem. A* **2023**, *127* (15), 3362–3371.

- (45) Balasubramanian, M.; Reynolds, A.; Blair, T. J.; Khalil, M. Probing Ultrafast Vibrational Dynamics of Intramolecular Hydrogen Bonds with Broadband Infrared Pump-Probe Spectroscopy. *Chem. Phys.* **2019**, *519*, 38–44.
- (46) Shirota, H. Intermolecular Vibrations and Diffusive Orientational Dynamics of C_s Condensed Ring Aromatic Molecular Liquids. *J. Phys. Chem. A* **2011**, *115* (50), 14262–14275.
- (47) Schwartz, M.; Duan, D.; Berry, R. J. Molecular Dynamics Study of Anisotropic Translational and Rotational Diffusion in Liquid Benzene. *J. Phys. Chem. A* **2005**, *109* (38), 8637–8641.
- (48) Dutt, G. B. Rotational Diffusion of Nondipolar Probes in Triton X-100 Micelles: Role of Specific Interactions and Micelle Size on Probe Dynamics. *J. Phys. Chem. B* **2002**, *106* (29), 7398–7404.
- (49) Sturlaugson, A. L.; Fruchey, K. S.; Fayer, M. D. Orientational Dynamics of Room Temperature Ionic Liquid/Water Mixtures: Water-Induced Structure. *J. Phys. Chem. B* **2012**, *116* (6), 1777–1787.
- (50) Sturlaugson, A. L.; Fruchey, K. S.; Lynch, S. R.; Aragon, S. R.; Fayer, M. D. Orientational and Translational Dynamics of Polyether/Water Solutions. *J. Phys. Chem. B* **2010**, *114* (16), 5350–5358.
- (51) Giammanco, C. H.; Wong, D. B.; Fayer, M. D. Water Dynamics in Divalent and Monovalent Concentrated Salt Solutions. *J. Phys. Chem. B* **2012**, *116* (46), 13781–13792.
- (52) Udagawa, T.; Yabushita, H.; Tanaka, H.; Kuwahata, K.; Tachikawa, M. Nuclear Quantum and H/D Isotope Effects on Intramolecular Hydrogen Bond in Curcumin. *Phys. Chem. Chem. Phys.* **2023**, 25 (23), 15798–15806.
- (53) Tan, H.-S.; Piletic, I. R.; Fayer, M. D. Orientational Dynamics of Water Confined on a Nanometer Length Scale in Reverse Micelles. *J. Chem. Phys.* **2005**, *122* (17), 174501.
- (54) Valentine, M. L.; Yin, G.; Oppenheim, J. J.; Dincă, M.; Xiong, W. Ultrafast Water H-Bond Rearrangement in a Metal—Organic Framework Probed by Femtosecond Time-Resolved Infrared Spectroscopy. J. Am. Chem. Soc. 2023, 145 (21), 11482–11487.
- (55) Hansen, B. K. V.; Winther, M.; Spanget-Larsen, J. Intramolecular Hydrogen Bonding. Spectroscopic and Theoretical Studies of Vibrational Transitions in Dibenzoylmethane Enol. *J. Mol. Struct.* **2006**, 790 (1), 74–79.
- (56) Etinski, M.; Ensing, B. Puzzle of the Intramolecular Hydrogen Bond of Dibenzoylmethane Resolved by Molecular Dynamics Simulations. *J. Phys. Chem. A* **2018**, 122 (28), 5945–5954.
- (57) Fournier, J. A.; Carpenter, W.; De Marco, L.; Tokmakoff, A. Interplay of Ion Water and Water Water Interactions within the Hydration Shells of Nitrate and Carbonate Directly Probed with 2D IR Spectroscopy. J. Am. Chem. Soc. 2016, 138 (30), 9634–9645.
- (58) De Marco, L.; Fournier, J. A.; Thamer, M.; Carpenter, W.; Tokmakoff, A. Anharmonic Exciton Dynamics and Energy Dissipation in Liquid Water from Two-Dimensional Infrared Spectroscopy. *J. Chem. Phys.* **2016**, *145* (9), 14.
- (59) Hamm, P.; Stock, G. Vibrational Conical Intersections as a Mechanism of Ultrafast Vibrational Relaxation. *Phys. Rev. Lett.* **2012**, 109, No. 173201.
- (60) Vlček, A., Jr.; Kvapilová, H.; Towrie, M.; Záliš, S. Electron-Transfer Acceleration Investigated by Time Resolved Infrared Spectroscopy. Acc. Chem. Res. 2015, 48 (3), 868–876.
- (61) Chuntonov, L. 2D-IR Spectroscopy of Hydrogen-Bond-Mediated Vibrational Excitation Transfer. *Phys. Chem. Chem. Phys.* **2016**, *18* (20), 13852–13860.
- (62) Elsaesser, T. Two-Dimensional Infrared Spectroscopy of Intermolecular Hydrogen Bonds in the Condensed Phase. *Acc. Chem. Res.* **2009**, 42 (9), 1220–1228.
- (63) Videla, P. E.; Foguel, L.; Vaccaro, P. H.; Batista, V. S. Proton-Tunneling Dynamics along Low-Barrier Hydrogen Bonds: A Full-Dimensional Instanton Study of 6-Hydroxy-2-Formylfulvene. *J. Phys. Chem. Lett.* **2023**, *14*, 6368–6375.
- (64) Carpenter, W. B.; Fournier, J. A.; Lewis, N. H. C.; Tokmakoff, A. Picosecond Proton Transfer Kinetics in Water Revealed with Ultrafast IR Spectroscopy. *J. Phys. Chem. B* **2018**, *122*, 2792–2802.
- (65) Berkelbach, T. C.; Lee, H.-S.; Tuckerman, M. E. Concerted Hydrogen-Bond Dynamics in the Transport Mechanism of the

Hydrated Proton: A First-Principles Molecular Dynamics Study. *Phys. Rev. Lett.* **2009**, 103 (23), No. 238302.

- (66) Biswas, R.; Tse, Y.-L. S.; Tokmakoff, A.; Voth, G. A. Role of Presolvation and Anharmonicity in Aqueous Phase Hydrated Proton Solvation and Transport. *J. Phys. Chem. B* **2016**, *120* (8), 1793–1804. (67) Tse, Y.-L. S.; Knight, C.; Voth, G. A. An Analysis of Hydrated Proton Diffusion in *Ab Initio* Molecular Dynamics. *J. Chem. Phys.* **2015**, *142* (1), No. 014104.
- (68) Laage, D.; Hynes, J. T. On the Molecular Mechanism of Water Reorientation. J. Phys. Chem. B 2008, 112 (45), 14230-14242.